Wen Yi, Iain M. Reid, Xianghui Xue, Joel P. Younger, Damian J. Murphy, Tingdi Chen, and Xiankang Dou
Response of neutral mesospheric density to geomagnetic forcing
Geophysical Research Letters, 2017; 44(16):8647-8655

DOI: http://dx.doi.org/10.1002/2017GL074813

AGU PUBLICATIONS

Geophysical Research Letters

RESEARCH LETTER
10.1002/2017GL074813

Key Points:
- The neutral mesospheric density over Antarctica responds to recurrent geomagnetic activity
- A 13.5 day oscillation is observed in neutral mesospheric density from 85 to 95 km over Antarctica in the declining phase of solar cycle 24
- The 13.5 day periodic oscillation in dayside density has a high anticorrelation with periodic changes in the auroral electrojet index

Correspondence to:
I. M. Reid and X. Xue,
iain.reid@adelaide.edu.au;
xuexh@ustc.edu.cn

Citation:
Yi, W., I. M. Reid, X. Xue, J. P. Younger, D. J. Murphy, T. Chen, and X. Dou (2017), Response of neutral mesospheric density to geomagnetic forcing, *Geophys. Res. Lett.*, *44*, 8647–8655, doi:10.1002/2017GL074813.

Received 4 JUL 2017
Accepted 10 AUG 2017
Accepted article online 15 AUG 2017
Published online 26 AUG 2017

Response of neutral mesospheric density to geomagnetic forcing

Wen Yi[1,2,3], Iain M. Reid[3,4], Xianghui Xue[1,2,5], Joel P. Younger[3,4], Damian J. Murphy[6], Tingdi Chen[1,2], and Xiankang Dou[1]

[1]CAS Key Laboratory of Geospace Environment, Department of Geophysics and Planetary Sciences, University of Science and Technology of China, Hefei, China, [2]Mengcheng National Geophysical Observatory, School of Earth and Space Sciences, University of Science and Technology of China, Hefei, China, [3]School of Physical Sciences, University of Adelaide, Adelaide, South Australia, Australia, [4]ATRAD Pty Ltd., Thebarton, South Australia, Australia, [5]Synergetic Innovation Center of Quantum Information and Quantum Physics, University of Science and Technology of China, Hefei, China, [6]Australian Antarctic Division, Kingston, Tasmania, Australia

Abstract We report an analysis of the neutral mesosphere density response to geomagnetic activity from January 2016 to February 2017 over Antarctica. Neutral mesospheric densities from 85 to 95 km are derived using data from the Davis meteor radar (68.5°S, 77.9°E) and the Microwave Limb Sounder on the Aura satellite. Spectral and Morlet wavelet analyses indicate that a prominent oscillation with a periodicity of 13.5 days is observed in the mesospheric density during the declining phase of solar cycle 24 and is associated with variations in solar wind high-speed streams and recurrent geomagnetic activity. The periodic oscillation in density shows a strong anticorrelation with periodic changes in the auroral electrojet index. These results indicate that a significant decrease in neutral mesospheric density as the geomagnetic activity enhances.

1. Introduction

The middle and upper atmosphere can be disturbed by the upward momentum deposition of atmospheric waves, including planetary waves, tides, and gravity waves from lower atmosphere [e.g., *Salby*, 1984; *Fritts and Alexander*, 2003; *Forbes and Garrett*, 1979], as well as downward energy and momentum transport through magnetosphere-ionosphere-thermosphere (MIT) coupling [e.g., *Xu et al.*, 2011; *Lei et al.*, 2010]. A direct relationship between rotating solar coronal holes and the Earth's upper atmosphere with periodicities of 5, 7, 9, and 13.5 day oscillations in the thermosphere and ionosphere were originally reported by *Mlynczak et al.* [2008], *Lei et al.* [2008a, 2008c], and *Thayer et al.* [2008], as well as in subsequent studies including *Lei et al.* [2008b, 2011], *Crowley et al.* [2008], *Sojka et al.* [2009], *Chang et al.* [2009], *Pedatella et al.* [2010], *Tulasi Ram et al.* [2010], *Jiang et al.* [2014], and *Xu et al.* [2015]. However, the periodic oscillations observed in these studies are confined to the MIT system, with the mechanism considered to be Joule and particle heating of the thermosphere [e.g., *Jiang et al.*, 2014].

Geomagnetic activity can affect the polar middle atmosphere through the impact of energetic particle (protons, electrons, and rarely heavier ions) precipitation (EPP) on atmospheric chemistry [e.g., *Turunen et al.*, 2009; *Daae et al.*, 2012]. In particular, EPP can lead to the production of odd hydrogen (HO_x = H + OH + HO_2) and odd nitrogen (NO_x = N + NO + NO_2), both of which can cause the depletion of mesospheric ozone (O_3) [see, e.g., *Andersson et al.*, 2012, 2014a, 2014b, 2016; *Verronen et al.*, 2011, 2013; *Fytterer et al.*, 2015, 2016; *Turunen et al.*, 2016; *Zawedde et al.*, 2016]. These studies have found evidence of the impact of geomagnetic forcing on the composition of the mesosphere, especially mesospheric O_3. However, the expected related response of neutral mesospheric temperature and density to such geomagnetic forcing has never been found.

Accurate knowledge of neutral mesospheric density is essential for studying the dynamics and climate in this region, but continuous measurements of neutral mesospheric density are difficult to obtain, leading to relatively scarce data. Estimates of the ambipolar diffusion coefficient by meteor radar are sensitive to changes in atmospheric density and temperature, which provide methods to estimate neutral mesospheric density. In this paper, data from an Antarctic meteor radar from January 2016 to February 2017 are used to estimate neutral mesospheric density height profiles. We find that neutral mesospheric density shows

a clear response to geomagnetic activity and discuss a possible mechanism for this magnetosphere-mesosphere coupling.

2. Data and Method

An ATRAD meteor detection radar has been operated by the Australian Antarctic Division since 2005 at Davis Station (68.5°S, 77.9°E; magnetic latitude, 74.6°S), Antarctica. The Davis meteor radar operates at a frequency of 33 MHz with a peak power of 7.5 kW and transmits 3.6 km long, 4 bit complimentary coded circularly polarized pulses at a pulse repetition rate of 430 Hz [*Holdsworth et al*., 2004, 2008].

The typical meteor detection rate of the Davis meteor radar is 5000–15000 unambiguous underdense meteor echoes per day, with maximum count rates observed in the southern hemisphere summer (December/January) and minimum in winter (August/September) [e.g., *Reid et al*., 2006]. In order to avoid the possibility of excessive error in the height estimates of individual meteors, trail detections for this study were restricted to zenith angles of less than 60°. This reduced the usable detection rate to 4000–10,000 per day. In this study, we separate the meteor radar data into dayside (6:00–18:00 h local time) and nightside (18:00–6:00 h local time), offering the opportunity to explore any local time dependency.

The Microwave Limb Sounder (MLS) instrument is on board the Earth Observing System (EOS) Aura spacecraft, which was launched in 2004. MLS observes atmospheric thermal microwave emissions in five spectral regions from 115 GHz to 2.5 THz. Temperatures are retrieved from bands near the O_2 spectral lines at 118 GHz and 239 GHz [*Schwartz et al*., 2008]. Restricting Aura MLS temperature and geopotential height data (version 4) to within a 300 km radius of the Davis meteor radar resulted in two sets of MLS observations at approximately 10:00 h and 19:00 h universal time. The daily MLS temperature and geopotential height observations were divided into dayside (near 10:00 h UT) and nightside (near 19:00 h UT), averaged, and interpolated into 1 km bins between 85 and 95 km to produce temperature profiles using geometric heights obtained from geopotential heights [see, e.g., *Younger et al*., 2014, 2015].

Solar wind and geomagnetic activity was characterized by the hourly averaged solar wind speed observed by the Advanced Composition Explorer (ACE) satellite, the planetary magnetic activity index, *Kp*, the auroral electrojet index, *AE*, and the daily solar activity proxy, $F_{10.7}$.

3. Analysis

The ambipolar diffusion coefficient D describes the rate at which plasma diffuses in a neutral background and is a function of atmospheric temperature, T, and atmospheric pressure, P, (or atmospheric density, ρ) [see, e.g., *Younger et al*., 2014] as given by

$$\rho = 2.23 \times 10^{-4} K_0 \frac{T}{D}, \tag{1}$$

where K_0 is the ionic zero-field mobility. Following *Chilson et al*. [1996], *Hocking et al*. [1997], and *Cervera and Reid* [2000], K_0 is assumed to be $2.5 \times 10^{-4} \mathrm{m}^{-2}\mathrm{s}^{-1}\mathrm{V}^{-1}$. Using the relation given by equation (1), measurements of the temperature and ambipolar diffusion coefficient can be used to retrieve neutral mesospheric density [e.g., *Takahashi et al*., 2002].

The $\log_{10}D$ profiles derived from meteor radar are approximately linear with respect to altitude in the range of 85–95 km [see, e.g., *Yi et al*., 2016], which indicates that the ambipolar diffusion mainly governs the evolution of meteor trails in this region [see, e.g., *Younger et al*., 2014]. To improve the accuracy of the height profile of D, an outlier rejection was applied, in which diffusion coefficients of more than two standard deviations from the mean were discarded, and a new mean was calculated from the remaining estimates of each 1 km height bin. Values of D and MLS temperature from 85 to 95 km were then to estimate the dayside and nightside neutral mesospheric density using equation (1).

The dayside and nightside densities estimated from the Davis meteor radar show a dominant annual variation, with a maximum during spring (November) and a minimum during winter (June). In this study, we focus on the shorter term periodic variabilities in mesospheric density, and so we remove seasonal variations to obtain the residual of the mesospheric neutral density. Observations of long-term changes,

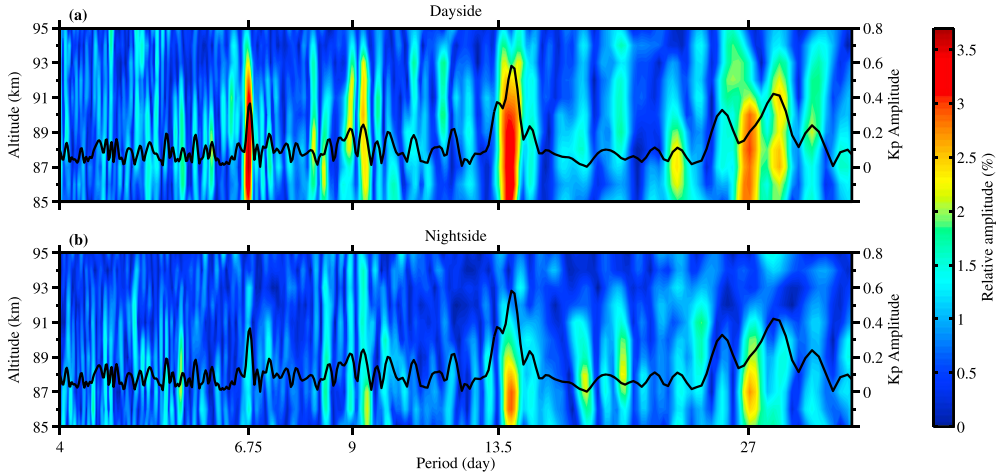

Figure 1. Contour of Lomb-Scargle spectral [see, e.g., *Lomb*, 1976; *Scargle*, 1982] amplitudes of (a) dayside and (b) nightside relative residual density as a function of altitude and period, from January 2016 to February 2017. The color bar indicates the percentage amplitude of the density residual to the mean density from January 2016 to February 2017. The Lomb-Scargle Periodogram of the simutaneous *Kp* index is also superimposed (solid line, right axis).

such as seasonal variations and solar cycle variations of neutral mesospheric density, will be detailed in subsequent work.

4. Results

As shown in Figure 1a, predominant spectral peaks in dayside density can be found at the periods of 27, 13.5, 9, and 6.75 days. These correspond to peaks in the spectra of the *Kp* index. It is interesting to note that these periodic oscillations in dayside density are more evident at lower altitudes and have largely disappeared above 92 km. As Figure 1b shows, the periodicities of 27, 13.5, and 9 day oscillations are also present in the nightside density but seem to be confined to heights below about 89 km.

Note that we only examine the 13.5 day periodicity in this study, although periodicities of 6.75, 9, and 27 days are also present in the neutral mesospheric density during this period. This is because the 6.75 and 9 day periodicities are present but relatively weak, and the 27 day periodicity is present in both geomagnetic activity and solar EUV radiation, which makes it difficult to separate the impact of the different forcing.

The Morlet wavelet [see, e.g., *Torrence and Compo*, 1998; *Liu et al*., 2007] results in Figures 2a and 2b show that the 13.5 day oscillation is the most prominent feature in dayside density and is almost always present around days 280(2016)–15(2017). The 13.5 day periodic variation is weaker in nightside density than in dayside density, but it is still clearly evident in some periods, such as around days 275–305 in 2016.

The peak height of the meteor detection distribution can serve as a proxy for the height of a constant neutral mesospheric density surface and so can provide insight into planetary wave activity [see, e.g., *Stober et al*., 2012]. The wavelet spectral power of peak height in Figures 2c and 2d shows similar 13.5 day periodic oscillations with density, and the time occurrence of this periodic oscillation in peak height is consistent with the density. Similar to the nightside density, the 13.5 day oscillation in the nightside peak height is weaker than in dayside. However, it should be noted that all of disturbances in nightside peak height seem to be weaker than in dayside. The presence of a 13.5 day oscillation in peak height, which depends directly on density, can be used to exclude the possibility that the geomagnetic field and background plasma of ionospheric *D* region effects are influencing the density values obtained from ambipolar diffusion coefficient estimates [see, e.g., *Jones*, 1991; *Ceplecha et al*., 1998].

It should be noted that the 13.5 day oscillations were not present in MLS temperatures during the period of this study. *Lee et al*. [2013] found a direct relation between the strength of summertime high northern latitude *D* region VHF echo strength and high-speed solar wind streams in 2006 and 2008, but no response of a similar period in MLS temperature data. In their case, the echo strength is likely being enhanced by direct particle precipitation "illuminating" the turbulent structures, rather than a direct density response. A similar

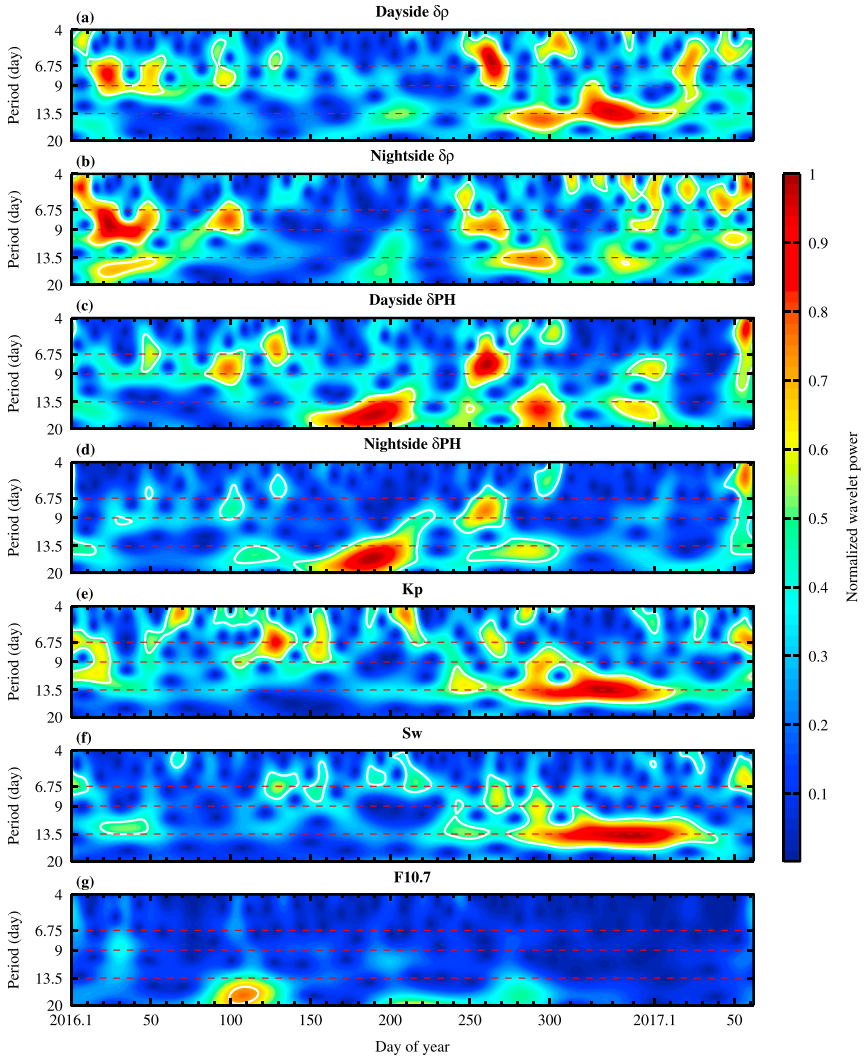

Figure 2. Morlet wavelet power spectra of the time series of the residual from (a) dayside and (b) nightside density at 87 km, the residual from (c) dayside and (d) nightside peak height, (e) *Kp*, (f) solar wind velocity, and (g) $F_{10.7}$ index from 2016 to February 2017. The white solid contours denote the regions of the wavelet spectrum above the 95% confidence level.

relationship between high northern latitude VHF radar echo occurrence and absorption has previously been suggested by *Czechowsky et al.* [1989].

From Figures 2e and 2f, we find that the time evolution of the 13.5 day oscillation in the density perturbations matches well with those of the solar wind speed and *Kp*. This indicates that the observed 13.5 day oscillations in the neutral mesospheric density are related to the variations of solar wind and recurrent geomagnetic activity. Finally, the wavelet spectral plot of $F_{10.7}$ in Figure 2g confirms again that the variations with a periodicity of 13.5 days in density are not present in the $F_{10.7}$ index during this period, and so we can exclude solar EUV flux effects as a direct driver of these oscillations.

The 27 day and harmonic periodicities of recurrent geomagnetic activities are caused by periodic high-speed solar wind streams originating from the average distribution of coronal holes in solar longitude [*Temmer et al.*, 2007; *Lei et al.*, 2008b]. It is interesting to note that the periodicity of 13.5 day is the strongest feature in our study. However, the 9 day oscillation is the strongest feature in solar cycle 23, especially in 2005 [e.g., *Lei et al.*, 2008a, 2008b, 2008c], while the 13.5 day oscillation is weak in solar cycle 23. *Xu et al.* [2015] compared the strength of 9 and 13.5 day oscillations in thermospheric density from 1967 to 2007 and found that only

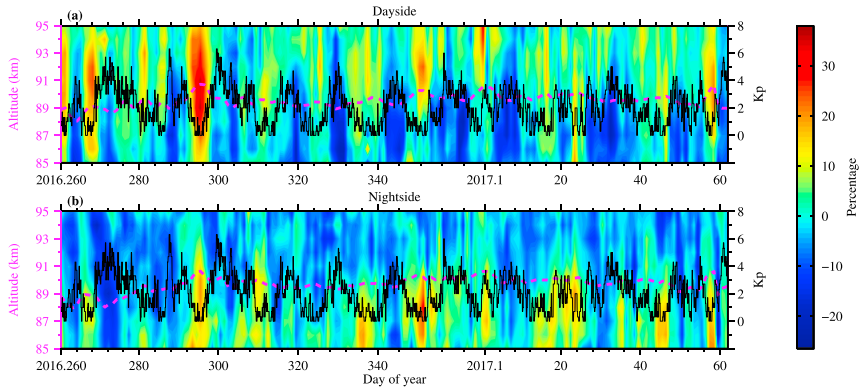

Figure 3. Davis meteor radar (a) dayside and (b) nightside density residual percentage as a function of time and height. The color bar indicates the percentage of residual density to the mean density during 260(2016)–62(2017). The magenta dashed line denotes the meteor peak height. The solid black line denotes the *Kp* values, corresponding to the right axis.

during 2003–2007 was the 9 day oscillation stronger than the 13.5 day oscillation, with the 13.5 day oscillation usually being stronger than the 9 day oscillation.

During the declining phase of a solar cycle and solar minimum, recurrent geomagnetic activity often occurs as a result of periodic forcing by high-speed solar wind streams and corotating interaction regions (CIRs) [*Tsurutani et al*., 2006]. The years of 2016 and 2017 lie just in the declining phase of solar cycle 24 as solar activity is weakening. The 13.5 day oscillation is the primary feature in periodic geomagnetic activity in this solar cycle and may be gradually strengthening as the minimum of solar cycle 24 approaches.

5. Discussion and Summary

Spectral analysis of the Davis meteor radar density from 85 to 95 km, shown in Figures 1 and 2, reveals that a 13.5 day oscillation is presents in mesospheric density and is associated with solar wind and recurrent geomagnetic activity. An outstanding question is how periodic variations of solar wind and geomagnetic activity are modulating neutral mesospheric density. As the 13.5 day osicllation in meospheric density is much more evident during days 260(2016)–62(2017) in the wavelet results in Figure 2, we limit our investigation to this period to further examine the relationship between mesosphreic density and *Kp*.

Note that there is a clear anticorrelation between density and *Kp* in Figure 3a, which is stronger at lower than higher altitudes. In addition, the dayside peak height also shows a rough anticorrelation with *Kp*. Furthermore, the 13.5 day periodic variation is clearly visible in dayside density and *Kp* after day 260 of 2016. The anticorrelation is not as obvious in the nightside density as in the dayside density, but is still present at times, such as the period around the days 260–275 in 2016, where there is a decrease in density as the geomagnetic activity enhances.

Numerous studies have reported an in-phase response of thermospheric density and temperature to periodic oscillations of geomagnetic activity [e.g., *Lei et al*., 2008a, 2008b, 2011; *Chang et al*., 2009; *Qian et al*., 2010; *Jiang et al*., 2014; *Xu et al*., 2015]. The mechanism driving these periodic oscillations is considered to be Joule and particle heating in the thermosphere [*Lei et al*., 2008a, 2008b; *Qian et al*., 2010; *Jiang et al*., 2014]. *Crowley et al*. [2008] reported an anticorrelation between the $\sum O/N_2$ ratio in thermosphere at high latitudes and geomagnetic activity and suggested the mechanism of uplifted molecular-rich air carried by upwelling winds driven by Joule and particle heating in the lower thermosphere. However, in our study, the antiphase response of density to periodic geomagnetic activity is present in the mesosphere and increases in magnitude with decreasing altitude.

The influence of Joule heating is confined to the lower thermosphere at low and middle latitudes [*Jiang et al*., 2014], with possible penetration down to the polar mesosphere during strong magnetic storms [*Sinnhuber et al*., 2012]. However, in our study, we found the neutral mesospheric density to be sensitive to both geomagnetic storms and small geomagnetic activity ($Kp < 3$). This may suggest another mechanism for the response of neutral mesospheric density to geomagnetic activity.

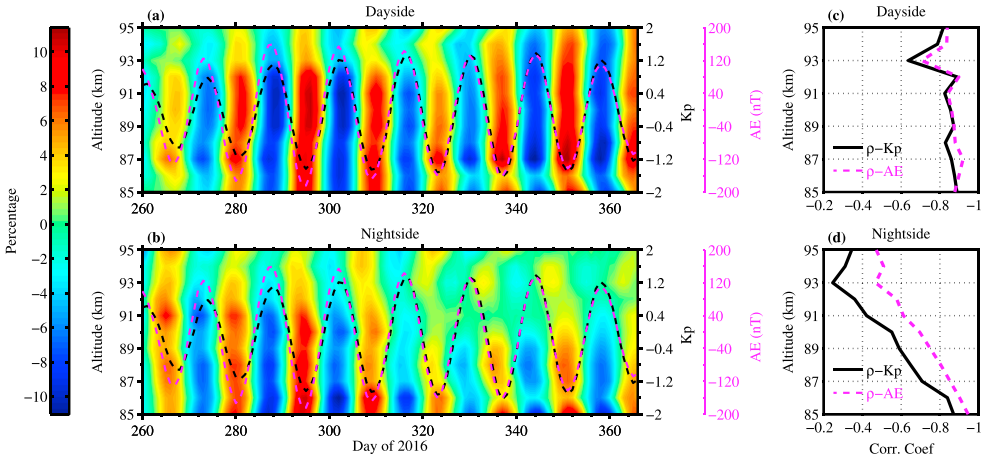

Figure 4. Density residual percentages of the (a) dayside and (b) nightside band-pass filtered at 13.5 days (10–16 days) with a mean density calculated for days 260–366 of 2016. The perturbations at 13.5 days in *Kp* (black dashed line) and *AE* index (magenta dashed line) obtained from the same band-pass filter are shown and correspond to the right-hand scale. Also shown are the correlation coefficients between the band-pass filter density and *Kp* (black solid lines), as well as *AE* index (magenta dashed line) in (c) dayside and (d) nightside.

To further examine this phenomenon, we applied a band-pass filter to the time series of mesospheric density and *Kp*, as well as the auroral electrojet index, *AE*, which is used to indicate the strength of energetic particle precipitation into the polar mesosphere, during days 260–366 in 2016. The band-pass filter is centered at the period of 13.5 days with lower and upper bounds of 10 and 16 days.

Figures 4a and 4b show clear anticorrelations between density and *Kp* and *AE* indices and also shows that the effects of geomagnetic activity have a local time dependency in that they are stronger in the dayside, rather than the nightside. Figure 4c shows that the correlations between mesospheric density oscillation and *Kp* and *AE* indices are quite strong, with a small decrease with increasing altitude, from −0.90 to −0.64 and from −0.92 to −0.71, respectively. However, Figure 4d shows that the anticorrelations between the nightside density and *Kp* and *AE* both show a substantial weakening with increasing altitude. In this case, the correlation coefficients between nightside density and *Kp* and *AE* decrease from −0.87 to −0.24 and from −0.94 to −0.46, respectively. Note that the correlation between nightside density and *AE* is obviously stronger than that with *Kp*. In addition, a slightly stronger correlation can be also found between the dayside density and *AE*. This indicates that the periodic oscillation in mesospheric neutral density has a stronger response to the auroral energetic particle precipitation than to geomagnetic activity.

Recent observations and modeling has indicated the significant impact of EPP driven by high-speed solar wind streams and CIRs [*Turunen et al*., 2009] on the chemistry of the mesosphere and lower thermosphere [e.g., *Sinnhuber et al*., 2012; *Andersson et al*., 2014b, 2016; *Fytterer et al*., 2015, 2016; *Turunen et al*., 2016]. These studies find that the most important processes are dissociation, dissociative ionization, and ionization of N_2, O_2, and O. These processes are followed by ion-chemistry formation of NO_x and HO_x, and a subsequent loss on the order of tens of percent of mesospheric O_3 at 70–80 km [*Andersson et al*., 2014b]. In addition, *Tsuda et al*. [2017] found a significant decrease in the Na density with an increase in the *AE* index due to the effects of EPP above 95 km in both northern and southern polar regions. These authors also note that mesospheric dynamics can be affected by a combination of Joule heating, chemical and radiative heating changes, and resultant changes in the interaction between the zonal mean flow, gravity wave propagation, and gravity wave breaking. It is well known that the absorption of solar ultraviolet (UV) radiation by O_3 is an important source of mesospheric heating and cooling, and changes to ozone concentration will significantly affect the local mesospheric temperature, as well as mesospheric density. The range of possible processes and their impacts are complex, but we can provide a simple possible explanation that is consistent with our results.

We propose the explanation that the periodic variation of the high-speed solar wind stream modulates a similar geomagnetic disturbance (shown in *Kp*) in the magnetosphere during the declining phase of a

solar cycle and solar minimum, which in turn leads to a similar variation in EPP (shown in *AE*). This can directly penetrate into the mesophere from the Earth's radiation belts, causing a depletion of mesospheric O_3 [e.g., *Andersson et al*., 2014b; *Fytterer et al*., 2015; *Turunen et al*., 2016]. This in turn would lead to the loss of radiative heating by O_3 absorption, leading to a temperature reduction, as well as a decrease in mesospheric density. This suggestion, although speculative, is consistent with both the anticorrelation between the geomagnetic activity and the neutral mesospheric density, and also with the strengthening response with decreasing altitude. It is also consistent with the local time dependence, having a stronger effect on the dayside density than the nightside density.

Electrons with energy levels of several keV-MeV can precipitate down to mesospheric regions with a geomagnetic latitudinal bands primarily between 55° and 75°S/N [e.g., *Andersson et al*., 2014a; *Fytterer et al*., 2015]. The Davis meteor radar is located just within this region. We note that we also find a similar response for densities determined using the Nippon/Norway Tromsø meteor radar [see, e.g., *Hall et al*., 2006; *Holmen et al*., 2016] (69.6°N, 19.2°E; magnetic latitude, 66.73°N) in the Arctic, but an absence of this effect for Mohe meteor radar observations in northern China [see, e.g., *Liu et al*., 2017] (53.5°N, 122.3°E, magnetic latitude, 44°N). This suggests a geomagnetic latitude dependence connected to the outer radiation belts which will be reported in detail in a following paper.

This is the first paper to report a response of neutral mesospheric density to geomagnetic forcing. It provides an important insight for future modeling work on the Earth's magnetosphere-thermosphere-mesosphere coupling. However, the actual mechanism of cooling due to EPP-induced ozone destruction has not been comprehensively proven and is left as an open question for the moment. Future observations and modeling are needed to more completely characterize the coupling process between geomagnetic activity and mesospheric density.

Acknowledgments

This work is supported by the National Natural Science Foundation of China (41774158, 41474129 and 41421063), the Chinese Academy of Sciences (KJCX2-EW-J01), the Youth Innovation Promotion Association of the Chinese Academy of Sciences (2011324), the Fundamental Research Fund for the Central Universities, and the China Scholarship Council. We also acknowledge support provided by the University of Adelaide and ATRAD Pty Ltd, and the provision of Davis meteor radar data by the Australian Antarctic Division. Operation of the Davis meteor radar was supported under Australian Antarctic Science project 4025. We thank the NASA EOS Aura MLS team for providing free access to their data. The MATLAB wavelet analysis software was provided by C. Torrence and G. Compo and is available at URL http://paos.colorado.edu/research/wavelets/software.html, and a rectified wavelet analysis software was provided by *Liu et al*. [2007] and is available at URL http://ocgweb.marine.usf.edu/~liu/wavelet.html. Aura/MLS data are available from http://disc.sci.gsfc.nasa.gov/Aura/data-holdings/MLS. The solar wind speed, *Kp*, *AE*, and $F_{10.7}$ data were obtained from the Goddard Space Flight Centre/Space Physics Data Facility (GSFC/SPDF) OMNIWeb interface (https://omniweb.gsfc.nasa.gov/ow.html). Meteor radar data are available from the University of Adelaide and the Australian Antarctic Division upon request. The involvement of IMR and JPY was supported by ATRAD Pty Ltd.

References

Andersson, M. E., P. T. Verronen, S. Wang, C. J. Rodger, M. A. Clilverd, and B. R. Carson (2012), Precipitating radiation belt electrons and enhancements of mesospheric hydroxyl during 2004–2009, *J. Geophys. Res.*, *117*, D09304, doi:10.1029/2011JD017246.

Andersson, M. E., P. T. Verronen, C. J. Rodger, M. A. Clilverd, and A. Seppälä (2014a), Missing driver in the Sun–Earth connection from energetic electron precipitation impacts mesospheric ozone, *Nat. Commun.*, *5*, 5197, doi:10.1038/ncomms6197.

Andersson, M. E., P. T. Verronen, C. J. Rodger, M. A. Clilverd, and S. Wang (2014b), Longitudinal hotspots in the mesospheric OH variations due to energetic electron precipitation, *Atmos. Chem. Phys.*, *14*(2), 1095–1105, doi:10.5194/acp-14-1095-2014.

Andersson, M. E., P. T. Verronen, D. R. Marsh, S. M. Päivärinta, and J. M. C. Plane (2016), WACCM-D—Improved modeling of nitric acid and active chlorine during energetic particle precipitation, *J. Geophys. Res. Atmos.*, *121*, 10,328–10,341, doi:10.1002/2015JD024173.

Ceplecha, Z., et al. (1998), Meteor phenomena and bodies, *Space Sci. Rev.*, *84*, 327–471, doi:10.1023/A:1005069928850.

Cervera, M. A., and I. M. Reid (2000), Comparison of atmospheric parameters derived from meteor observations with CIRA, *Radio Sci.*, *35*, 833–843.

Chang, L. C., J. P. Thayer, J. Lei, and S. E. Palo (2009), Isolation of the global MLT thermal response to recurrent geomagnetic activity, *Geophys. Res. Lett.*, *36*, L15813, doi:10.1029/2009GL039305.

Chilson, P. B., P. Czechowsky, and G. Schmidt (1996), A comparison of ambipolar diffusion coefficients in meteor trains using VHF radar and UV lidar, *Geophys. Res. Lett.*, *23*, 2745–2748.

Crowley, G., A. Reynolds, J. P. Thayer, J. Lei, L. J. Paxton, A. B. Christensen, Y. Zhang, R. R. Meier, and D. J. Strickland (2008), Periodic modulations in thermospheric composition by solar wind high speed streams, *Geophys. Res. Lett.*, *35*, L21106, doi:10.1029/2008GL035745.

Czechowsky, P., I. M. Reid, R. Rüster, and G. Schmidt (1989), VHF radar echoes observed in the summer and winter polar mesosphere over Andøya, Norway, *J. Geophys. Res.*, *94*(D4), 5199–5217, doi:10.1029/JD094iD04p05199.

Daae, M., P. Espy, H. Nesse Tyssøy, D. Newnham, J. Stadsnes, and F. Søraas (2012), The effect of energetic electron precipitation on middle mesospheric night-time ozone during and after a moderate geomagnetic storm, *Geophys. Res. Lett.*, *39*, L21811, doi:10.1029/2012GL053787.

Forbes, J. M., and H. B. Garrett (1979), Theoretical studies of atmospheric tides, *Rev. Geophys. Space Phys.*, *17*, 1951–1981.

Fritts, D. C., and M. J. Alexander (2003), Gravity wave dynamics and effects in the middle atmosphere, *Rev. Geophys.*, *41*(1), 1003, doi:10.1029/2001RG000106.

Fytterer, T., M. L. Santee, M. Sinnhuber, and S. Wang (2015), The 27 day solar rotational effect on mesospheric nighttime OH and O_3 observations induced by geomagnetic activity, *J. Geophys. Res. Space Physics*, *120*, 7926–7936, doi:10.1002/2015JA021183.

Fytterer, T., S. Bender, U. Berger, H. Nieder, M. Sinnhuber, and J. M. Wissing (2016), Model studies of short-term variations induced in trace gases by particle precipitation in the mesosphere and lower thermosphere, *J. Geophys. Res. Space Physics*, *121*, 10,431–10,447, doi:10.1002/2015JA022291.

Hall, C. M., T. Aso, M. Tsutsumi, J. Höffner, F. Sigernes, and D. A. Holdsworth (2006), Neutral air temperatures at 90 km and 70°N and 78°N, *J. Geophys. Res.*, *111*, D14105, doi:10.1029/2005JD006794.

Hocking, W. K., T. Thayaparan, and J. Jones (1997), Meteor decay times and their use in determining a diagnostic mesospheric temperature-pressure parameter: Methodology and one year of data, *Geophys. Res. Lett.*, *24*, 2977–2980.

Holdsworth, D. A., I. M. Reid, and M. A. Cervera (2004), Buckland Park all-sky interferometric meteor radar, *Radio Sci.*, *39*, RS5009, doi:10.1029/2003RS003014.

Holdsworth, D. A., D. J. Murphy, I. M. Reid, and R. J. Morris (2008), Antarctic meteor observations using the Davis MST and meteor radars, *Adv. Space Res.*, *42*(1), 143–154, doi:10.1016/j.asr.2007.02.037.

Holmen, S. E., C. M. Hall, and M. Tsutsumi (2016), Neutral atmosphere temperature trends and variability at 90 km, 70°N, 19°E, 2003–2014, *Atmos. Chem. Phys.*, *16*, 7853–7866.

Jiang, G., W. Wang, J. Xu, J. Yue, A. G. Burns, J. Lei, and J. M. Rusell III (2014), Responses of the lower thermospheric temperature to the 9 day and 13.5 day oscillations of recurrent geomagnetic activity, *J. Geophys. Res. Space Physics*, *119*, 4841–4859, doi:10.1002/2013JA019406.

Jones, W. (1991), Theory of diffusion of meteor trains in the geomagnetic field, *Planet. Space Sci.*, *39*(9), 1283–1288, doi:10.1016/0032-0633(91)90042-9.

Lee, Y.-S., S. Kirkwood, G. G. Shepherd, Y.-S. Kwak, and K.-C. Kim (2013), Long-periodic strong radar echoes in the summer polar *D* region correlated with oscillations of high-speed solar wind streams, *Geophys. Res. Lett.*, *40*, 4160–4164, doi:10.1002/grl.50821.

Lei, J., J. P. Thayer, J. M. Forbes, E. K. Sutton, and R. S. Nerem (2008a), Rotating solar coronal holes and periodic modulation of the upper atmosphere, *Geophys. Res. Lett.*, *35*, L10109, doi:10.1029/2008GL033875.

Lei, J., J. P. Thayer, J. M. Forbes, E. K. Sutton, R. S. Nerem, M. Temmer, and A. M. Veronig (2008b), Global thermospheric density variations caused by high-speed solar wind streams during the declining phase of solar cycle 23, *J. Geophys. Res.*, *113*, A11303, doi:10.1029/2008JA013433.

Lei, J., J. P. Thayer, J. M. Forbes, Q. Wu, C. She, W. Wan, and W. Wang (2008c), Ionosphere response to solar wind high-speed streams, *Geophys. Res. Lett.*, *35*, L19105, doi:10.1029/2008GL035208.

Lei, J., J. P. Thayer, A. G. Burns, G. Lu, and Y. Deng (2010), Wind and temperature effects on thermosphere mass density response to the November 2004 geomagnetic storm, *J. Geophys. Res.*, *115*, A05303, doi:10.01029/02009JA014754.

Lei, J., J. P. Thayer, W. Wang, and R. L. McPherron (2011), Impact of CIR storms on thermosphere density variability during the solar minimum of 2008, *Sol. Phys.*, *274*(1), 427–437, doi:10.1007/s11207-010-9563-y.

Liu, L. B., H. X. Liu, H. J. Le, Y. D. Chen, Y. Y. Sun, B. Q. Ning, L. H. Hu, W. X. Wan, N. Li, and J. G. Xiong (2017), Mesospheric temperatures estimated from the meteor radar observations at Mohe, China, *J. Geophys. Res. Space Physics*, *122*, 2249–2259, doi:10.1002/2016JA023776.

Liu, Y., X. S. Liang, and R. H. Weisberg (2007), Rectification of the bias in the wavelet power spectrum, *J. Atmos. Oceanic Technol.*, *24*(12), 2093–2102.

Lomb, N. R. (1976), Least-squares frequency analysis of unequally spaced data, *Astrophys. Space Sci.*, *39*, 447–462.

Mlynczak, M. G., F. J. Martin-Torres, C. J. Mertens, B. T. Marshall, R. E. Thompson, J. U. Kozyra, E. E. Remsberg, L. L. Gordley, J. M. Russell III, and T. Woods (2008), Solarterrestrial coupling evidenced by periodic behavior in geomagnetic indexes and the infrared energy budget of the thermosphere, *Geophys. Res. Lett.*, *35*, L05808, doi:10.1029/2007GL032620.

Pedatella, N. M., J. Lei, J. P. Thayer, and J. M. Forbes (2010), Ionosphere response to recurrent geomagnetic activity: Local time dependency, *J. Geophys. Res.*, *115*, A02301, doi:10.1029/2009JA014712.

Qian, L., S. C. Solomon, and M. G. Mlynczak (2010), Model simulation of thermospheric response to recurrent geomagnetic forcing, *J. Geophys. Res.*, *115*, A10301, doi:10.1029/2010JA015309.

Reid, I. M., D. A. Holdsworth, R. J. Morris, D. J. Murphy, and R. A. Vincent (2006), Meteor observations using the Davis mesosphere-stratosphere-troposphere radar, *J. Geophys. Res.*, *111*, A05305, doi:10.1029/2005JA011443.

Salby, M. L. (1984), Survey of planetary-scale traveling waves: The state of theory and observations, *Rev. Geophys.*, *22*(2), 209–236, doi:10.1029/RG022i002p00209.

Scargle, J. D. (1982), Studies in astronomical time series analysis. II. Statistical aspects of spectral analysis of unevenly spaced data, *Astrophys. J.*, *263*, 835–853.

Schwartz, M. J., A. Lambert, G. L. Manney, W. G. Read, and N. J. Livesey (2008), Validation of the Aura Microwave Limb Sounder temperature and geopotential height measurements, *J. Geophys. Res.*, *113*, D15S11, doi:10.1029/2007JD008783.

Sinnhuber, M., H. Nieder, and N. Wieters (2012), Energetic particle precipitation and the chemistry of the mesosphere/lower thermosphere, *Surv. Geophys.*, *33*, 1281–1334, doi:10.1007/s10712-012-9201-3.

Stober, G., C. Jacobi, V. Matthias, P. Hoffmann, and M. Gerding (2012), Neutral air density variations during strong planetary wave activity in the mesopause region derived from meteor radar observations, *J. Atmos. Sol. Terr. Phys.*, *74*, 55–63.

Sojka, J. J., R. L. McPherron, A. P. van Eyken, M. J. Nicolls, C. J. Heinselman, and J. D. Kelly (2009), Observations of ionospheric heating during the passage of solar coronal hole fast streams, *Geophys. Res. Lett.*, *36*, L19105, doi:10.1029/2009GL039064.

Takahashi, H., T. Nakamura, T. Tsuda, R. A. Buriti, and D. Gobbi (2002), First measurement of atmospheric density and pressure by meteor diffusion coefficient and airglow OH temperature in the mesopause region, *Geophys. Res. Lett.*, *29*(8), 6-1–6-4, doi:10.1029/2001GL014101.

Temmer, M., B. Vršnak, and A. M. Veronig (2007), Periodic appearance of coronal holes and the related variation of solar wind parameters, *Sol. Phys.*, *241*, 371–383.

Thayer, J. P., J. Lei, J. M. Forbes, E. K. Sutton, and R. S. Nerem (2008), Thermospheric density oscillations due to periodic solar wind high-speed streams, *J. Geophys. Res.*, *113*, A06307, doi:10.1029/2008JA013190.

Tsuda, T. T., T. Nakamura, M. K. Ejiri, T. Nishiyama, K. Hosokawa, T. Takahashi, J. Gumbel, and J. Hedin (2017), Statistical investigation of Na layer response to geomagnetic activity using resonance scattering measurements by Odin/OSIRIS, *Geophys. Res. Lett.*, *44*, 5943–5950, doi:10.1002/2017GL072801.

Tsurutani, B. T., et al. (2006), Corotating solar wind streams and recurrent geomagnetic activity: A review, *J. Geophys. Res.*, *111*, A07S01, doi:10.1029/2005JA011273.

Turunen, E., P. T. Verronen, A. Seppälä, C. J. Rodger, M. A. Clilverd, J. Tamminen, and T. Ulich (2009), Impact of different energies of precipitating particles on NOx generation in the middle and upper atmosphere during geomagnetic storms, *J. Atmos. Sol. Terr. Phys.*, *71*(10–11), 1176–1189, doi:10.1016/j.jastp.2008.07.005.

Turunen, E., A. Kero, P. T. Verronen, Y. Miyoshi, S. I. Oyama, and S. Saito (2016), Mesospheric ozone destruction by high-energy electron precipitation associated with pulsating aurora, *J. Geophys. Res. Atmos.*, *121*, 11,852–11,861, doi:10.1002/2016JD025015.

Torrence, C., and G. P. Compo (1998), A practical guide to wavelet analysis, *Bull. Am. Meteorol. Soc.*, *79*, 61–78.

Tulasi Ram, S., J. Lei, S.-Y. Su, C. H. Liu, C. H. Lin, and W. S. Chen (2010), Dayside ionospheric response to recurrent geomagnetic activity during the extreme solar minimum of 2008, *Geophys. Res. Lett.*, *37*, L02101, doi:10.1029/2009GL041038.

Verronen, P. T., C. J. Rodger, M. A. Clilverd, and S. Wang (2011), First evidence of mesospheric hydroxyl response to electron precipitation from the radiation belts, *J. Geophys. Res.*, *116*, D07307, doi:10.1029/2010JD014965.

Verronen, P. T., M. E. Andersson, C. J. Rodger, M. A. Clilverd, S. Wang, and E. Turunen (2013), Comparison of modeled and observed effects of radiation belt electron precipitation on mesospheric hydroxyl and ozone, *J. Geophys. Res. Atmos.*, *118*, 11,419–11,428, doi:10.1002/jgrd.50845.

Xu, J., W. Wang, J. Lei, E. K. Sutton, and G. Chen (2011), The effect of periodic variations of thermospheric density on CHAMP and GRACE orbits, *J. Geophys. Res.*, *116*, A02315, doi:10.1029/2010JA015995.

Xu, J., W. Wang, S. Zhang, X. Liu, and W. Yuan (2015), Multiday thermospheric density oscillations associated with variations in solar radiation and geomagnetic activity, *J. Geophys. Res. Space Physics*, *120*, 3829–3846, doi:10.1002/2014JA020830.

Yi, W., X. Xue, J. Chen, X. Dou, T. Chen, and N. Li (2016), Estimation of mesopause temperatures at low latitudes using the Kunming meteor radar, *Radio Sci.*, *51*, 130–141, doi:10.1002/2015RS005722.

Younger, J. P., C. S. Lee, I. M. Reid, R. A. Vincent, Y. H. Kim, and D. J. Murphy (2014), The effects of deionization processes on meteor radar diffusion coefficients below 90 km, *J. Geophys. Res. Atmos.*, *119*, 10,027–10,043, doi:10.1002/2014JD0217.

Younger, J. P., I. M. Reid, R. A. Vincent, and D. J. Murphy (2015), A method for estimating the height of a mesospheric density level using meteor radar, *Geophys. Res. Lett.*, *42*, 6106–6111, doi:10.1002/2015GL065066.

Zawedde, A. E., H. N. Tyssøy, R. Hibbins, P. J. Espy, L. K. G. Ødegaard, M. I. Sandanger, and J. Stadsnes (2016), The impact of energetic electron precipitation on mesospheric hydroxyl during a year of solar minimum, *J. Geophys. Res. Space Physics*, *121*, 5914–5929, doi:10.1002/2016JA022371.